OPTRO2016-022

LONG WAVE INFRARED TYPE II SUPERLATTICE DETECTOR

L. Langof[(1)] , E. Avnon[(1)], Y. Benny[(1)], A. Fraenkel[(1)], A. Glozman[(1)], E. Hojman[(1)], E. Ilan[(1)], E. Kahanov[(1)], O Klin[(1)], P. C. Klipstein[(1)], L. Krasovitski[(1)], I. Lukomsky[(1)], M. Nitzani[(1)], L. Shkedy[(1)], I. Shtrichman[(1)], N. Snapi[(1)], R. Talmor[(1)], A.Tuito[(2)], S. Vaserman[(1)], and E. Weiss[(1)]

(1)SemiConductor Devices P.O. Box 2250, Haifa 31021, Israel, Email: lidia_langof@scd.co.il
(2)Israel MOD, Email: avit000@gmail.com

KEYWORDS: LWIR, T2SL, superlattice, pBp, XBp, InAs/GaSb, Focal Plane Array

ABSTRACT

SCD has developed a range of advanced infrared detectors based on III-V semiconductor heterostructures grown on GaSb. The XB*n*/XB*p* family of barrier detectors enables diffusion limited dark currents comparable with $Hg_xCd_{1-x}Te$ Rule-07 and high quantum efficiencies. SCD's XB*p* type II superlattice (T2SL) detector contains InAs/GaSb and InAs/AlSb T2SLs, and was designed for the long wave infrared (LWIR) atmospheric window using **k·p** based modeling of the energy bands and photo-response. Wafers are grown by molecular beam epitaxy and are fabricated into Focal Plane Array (FPA) detectors using standard FPA processes, including wet and dry etching, indium bump hybridization, under-fill, and back-side polishing. The detector goes by the name of "Pelican-D LW", and has a format of 640 × 512 pixels with a pitch of 15 µm. The FPA has a QE above 50%, a cut-off wave length of ~9.5 µm, and operates at 78K with background limited performance and good stability. Pelican-D LW has a pixel operability above 99% and a residual non uniformity (RNU) of better than 0.02%. It uses a new digital read-out integrated circuit, and the complete detector closely follows the configuration of SCD's MWIR Pelican-D detector.

1. INTRODUCTION

In a pioneering article[1] entitled "a new semiconductor superlattice" published in 1977, Sai-Halasz, Tsu and Esaki proposed that a superlattice based on alternating layers of InAs and GaSb would exhibit rather unique properties, including a zero bandgap at a critical value of the layer thicknesses. In this respect, the new

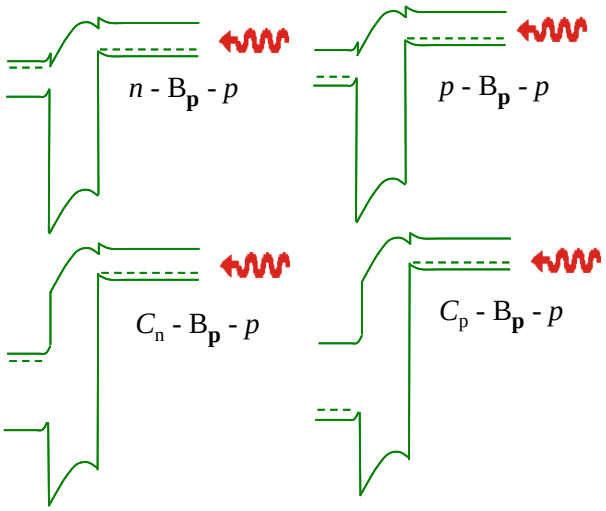

Figure 1. The four contact configurations of an XB_pp detector under an applied bias. The contact is on the left of the barrier

superlattice bore a close relationship with the alloy, $Hg_xCd_{1-x}Te$, where the bandgap vanishes at a critical value of the composition parameter, x. $Hg_xCd_{1-x}Te$ has become one of the most widely used tunable infrared detector materials, because it is a versatile technology that can match the characteristic photon wavelength of most infrared applications. On the other hand, InAs/GaSb superlattices, also known as type II superlattices (T2SLs), have only recently been considered to be a viable alternative technology to $Hg_xCd_{1-x}Te$, due to the more challenging crystal growth that is required. T2SLs must be grown by molecular beam epitaxy (MBE), which has taken longer to mature to a viable commercial production tool than the liquid phase epitaxy technique that is used most widely in the production of $Hg_xCd_{1-x}Te$ detector arrays. An important factor driving T2SL development, however, is that commercial 3" or 4" GaSb substrates can be used for their growth, while smaller and more expensive CdZnTe substrates must be used for the highest quality $Hg_xCd_{1-x}Te$.

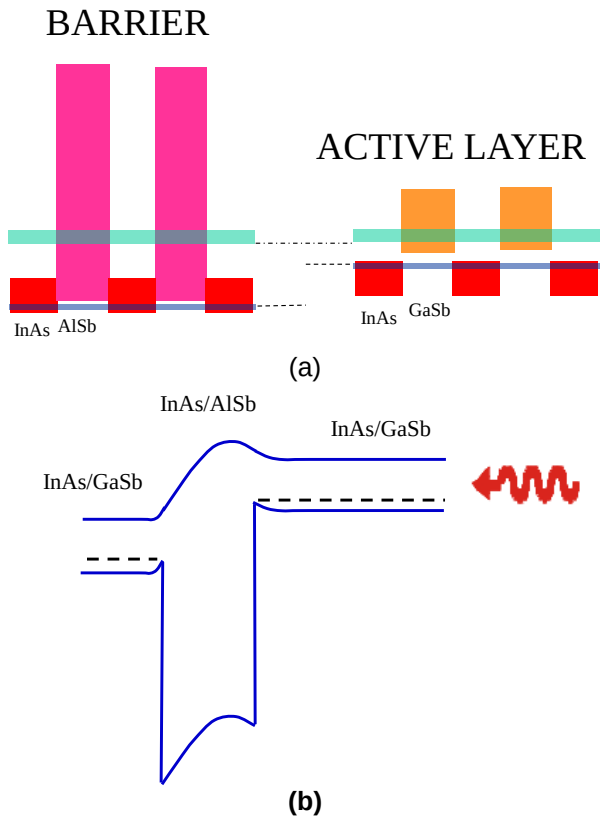

Figure 2. (a) Alignment between mini-bands in the active and barrier layers of a T2SL XBp device, super-imposed on the band gaps of InAs, GaSb and AlSb (b) Schematic profile of band edges in an operating pB_pp device, based on the mini-bands shown in (a)

Yet two more technological hurdles still had to be overcome, before T2SL technology began to look truly competitive. The first was the suppression of generation-recombination (G-R) limited dark current[2], which is absent in high quality $Hg_xCd_{1-x}Te$ photodiodes, and the second was device passivation. A novel barrier device, known as an XB*p* detector,[3,4] was developed at SCD, which contains two types of T2SL: InAs/GaSb for the photon absorbing or "active" layer and InAs/AlSb for the barrier layer. All T2SLs are doped *p*-type which ensures that the depletion layer is confined to the wide bandgap barrier layer. A depiction of four configurations of the XB*p* architecture at operating bias[5] is shown in Figure 1. All configurations have the same arrangement for the active and barrier layers, but different band alignments or doping types for the contact layer. G-R current occurs in the depleted barrier layer through mid-gap Shockley-Read-Hall (SRH) traps with an activation energy close to half of its bandgap. Since this bandgap is more than twice that of the active layer, the G-R current is negligible compared to the diffusion current coming out of the active layer. For this current, the activation energy is equal to the full active layer bandgap, since all SRH traps are occupied[5]. In this work it will be shown that the dark current in a T2SL XB*p* device is within one order of magnitude of the Rule 07 value, which is the state of the art metric for $Hg_xCd_{1-x}Te$ photodiodes[6].

The second technological hurdle that had to be overcome was a reliable passivation treatment of the processed XB*p* devices, which is compatible with all of the standard FPA processes, including wet and dry etching, indium bump hybridization, glue under-fill, and back-side polishing. The development of this passivation at SCD is the final step that has enabled the fabrication of long wave infrared (LWIR) T2SL FPAs with a performance comparable to high quality $Hg_xCd_{1-x}Te$ FPAs. The design and performance of these FPAs is the subject of this paper.

In section 2, the implementation of the XB*p* architecture in a LWIR T2SL device is presented, and theoretical predictions are compared with experimental measurements of dark current and quantum efficiency (QE) in test devices. The next section introduces the key parameters of SCD's new 15 µm pitch, 640 × 512 read-out integrated circuit (ROIC) designed to operate with XB*p*

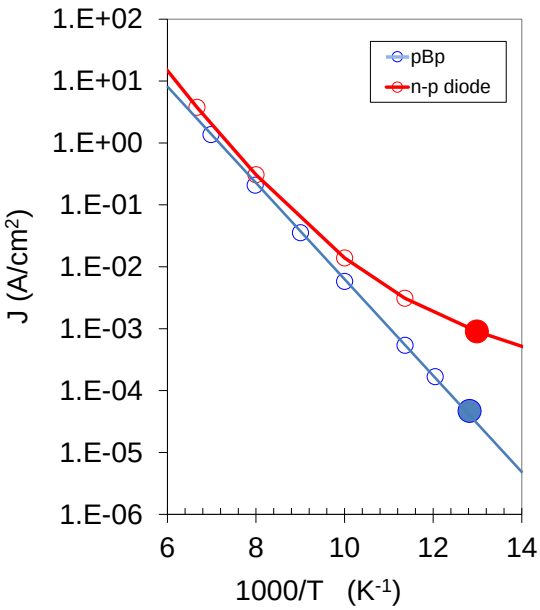

Figure 3. Log J_{dark} vs. 1000/T in pB_pp barrier device (bias = 0.6V) and n-p diode (bias = 0.1V), each with an InAs/GaSb active layer bandgap wavelength of λ_G~10 µm (mesa area = 100×100 µm²)

devices (equivalent polarity to *n*-on-*p* photo-diodes). The radiometric characteristics of the new FPA are presented in section 4, and conclusions are summarized in section 5

2. DESIGN AND PERFORMANCE OF T2SL BARRIER DEVICES

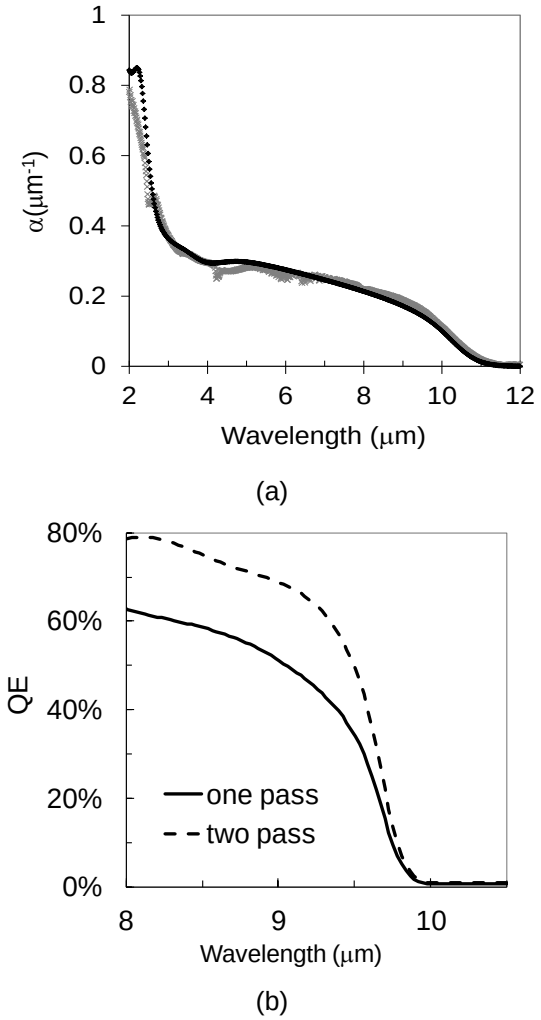

Figure 4. (a) Measured (grey line) and calculated (black line) absorption coefficient spectra for a 14.4/7.2 InAs/GaSb T2SL (dimensions in monolayers) and (b) calculated spectral response (quantum efficiency) for a XB$_p$p detector with a 4.5 μm thick AL made from a 13.8/7 InAs/GaSb T2SL when none of the LWIR radiation (solid line) or 80% of the LWIR radiation (dashed line) is reflected back from the contact for a second pass through the AL.

Figure 2(a) shows a schematic band structure for the barrier layer and active layer of an XB*p* device based on InAs/AlSb and InAs/GaSb T2SLs, respectively. In (b) the edges of the mini-bands shown in (a) are sketched for an operating *p*B$_p$*p* device, where all layers are doped *p*-type. The advantage of the barrier device is demonstrated in Figure 3, which compares a standard LWIR *n*-on-*p* diode based solely on InAs/GaSb and operating at a bias of 0.1V, with a LWIR *p*B$_p$*p* device based on the design in Figure 2, and operating at a bias of 0.6V. Both devices have an active layer band gap wavelength close to 10 μm. The barrier device (blue line) is diffusion limited down to 77K, while the diode (red line) is G-R limited at this temperature, with a dark current over 20× larger. The dark current in the barrier device of Figure 3 and in all of our XB*p* test devices is within one order of magnitude of $Hg_xCd_{1-x}Te$ Rule-07[7]

It is now shown how we are able to simulate the full spectral response for an FPA made from the *p*B$_p$*p* device shown in Figure 2, if the thickness of the InAs and GaSb layers in the T2SL period are known. This allows us to design the superlattices inside the structure correctly, prior to MBE growth. The simulation is based on a **k · p** treatment and optical transfer matrix (OTM) calculation recently reported elsewhere[8]. While the OTM technique is fairly standard, the **k · p** treatment contains a number of innovations[9]. This treatment leads to a reduced number of fitting parameters compared to other approaches, namely two independent Luttinger parameters (of InAs), three interface parameters, the valence band offset and a parameter close to unity that is related to the interband momentum matrix element. The same two Luttinger parameters are used for all superlattices of the form InAs/X where X=GaSb or AlSb, so they only need to be determined once. The fitted values turn out to be very close to those determined by other workers. All other parameters used in the calculation are based on established spectroscopic, mechanical or X-ray data available in the literature.

Figure 4 (a) compares the full absorption spectrum calculated with the **k · p** model (black line) for a 14.4/7.2 InAs/GaSb LWIR T2SL (dimensions in monolayers, ML) with an experimental spectrum (grey line) for this T2SL. Both the absolute absorption coefficient and the main spectral features appear to be reproduced quite well, including the strong peak just above 2 μm. This peak is due to superlattice zone boundary transitions between HH_2 and E_1, and is discussed in detail in Ref. 9. It should be noted that the absorption edge of the T2SL is fairly broad unlike that for the MWIR T2SLs reported in Ref. 9. The reason for this is that a very low doped GaSb substrate was used to grow the LWIR T2SL, so

that an absorption measurement could be performed up to a wavelength of 12 µm without the need to thin the substrate. In contrast doped substrates were used for the MWIR T2SLs because these are sufficiently transparent in the shorter wavelength range. The doped substrates had a higher crystalline quality and for this reason the MWIR T2SLs exhibit a much smaller inhomogeneous broadening[9]. The LWIR T2SLs used to fabricate our *p*B$_p$*p* detectors are also grown on doped substrates and these T2SLs have a more abrupt absorption edge, as for the MWIR T2SLs. Most of the doped substrate is removed later on in the fabrication process.

Figure 4(b) shows an OTM calculation of the spectral response of a *p*B$_p$*p* detector with an antireflection coating (ARC) and a 4.5 µm thick AL based on a 13.8/7 InAs/GaSb T2SL with a cut-off wavelength close to 10 µm. The OTM calculation uses a T2SL absorption spectrum deduced from the **k · p** model with narrow inhomogeneous broadening appropriate to growth on doped substrates. Although the InAs/AlSb barrier layer makes no contribution to the detector response, the **k · p** treatment described above is also used to design the correct layer widths in the barrier layer of the grown device. Figure 4(b) shows curves for both a single pass device (solid line) and a two pass device (dashed line) in which 80% of the light impinging on the metal contact of the contact layer is reflected back for a second pass through the active layer. It has been assumed that there are no losses of photo-carriers due to recombination in the bulk or at the surfaces (internal QE = 100%). Under these conditions, the two pass detector is able to provide an average QE of ~70%, defined as the spectral response in Figure 4 (b) weighted by the 300K black body radiation spectrum and averaged from the cut-on of the LWIR atmospheric widow (~8 µm) to the detector cut-off wavelength of 9.5 µm. The corresponding value for the single pass device is ~50%. We show below that the single pass value can be realized in a FPA which was designed as a one pass detector.

3. 640 × 512/15 µm DIGITAL ROIC

The new ROIC has an architecture that closely follows that of the mature and successful MWIR Pelican D ROIC[10]. This approach was chosen due to the excellent performance expected in terms of readout noise, Residual Non Uniformity (RNU), power dissipation and frame rate. Another important incentive was to support our incumbent customers with fast integration into systems and cameras. Nevertheless, the new T2SL LWIR technology poses two important challenges for the ROIC design:

1. The device polarity requires a polarity inversion in the ROIC circuitry.
2. The higher photon flux compared with the MWIR imposes very short integration periods due to the limited area available for the integration capacitors. To overcome this problem we have implemented a high frame rate (up to 360Hz) with frame averaging (up to 8 frames) performed in the proximity electronics. This enables us to achieve an NETD value @ F/2.7 and 30Hz of less than 15mK.

Parameter	Value
Well Capacity	> 6Me$^-$
Noise Floor	< 1300e$^-$
ROIC RNU	< 0.025% of DR
Dynamic Range	5350
ADC Resolution	13 bit (> 7000 DL)
Maximum Frame Rate	360Hz
Input Clock Frequency	80MHz
Power Consumption	110mW @ 360Hz
Operating Temperature	Functional at room temperature Full performance at 77K
Windowing	Supported
Up/Down Readout	Supported
Integration modes	ITR, IWR

Table 1 Pelican-D LW ROIC performance

The ROIC was tested at room temperature and 77K and the results compared favorably with preliminary predictions. Table presents the measured performance.

4. PELICAN-D LW FPA

"Pelican-D LW" is the first in our new line of LWIR XB*p* FPAs manufactured at SCD. The detector is based on a 15 µm pitch, 640 × 512 FPA bonded to the new digital silicon ROIC, described above. The FPA has a nominal T2SL cut-off wavelength of 9.5µm. In the rest of this section, we present some of the key radiometric performance parameters of a Pelican-D LW FPA measured after integration into a Detector-Dewar-Cooler (DDC) assembly. Dark current was measured in a laboratory Dewar, for this FPA, and several others with different cut-off wavelengths.

Figure 5 shows the FPA dark current distribution at 78K for 5 FPAs with cut-off wavelengths spanning the nominal value of 9.5µm. The median value for a cut-off of 9.4µm is close to 100pA and the distribution is quite narrow with a full width at half maximum of only ~6% of the median value. The

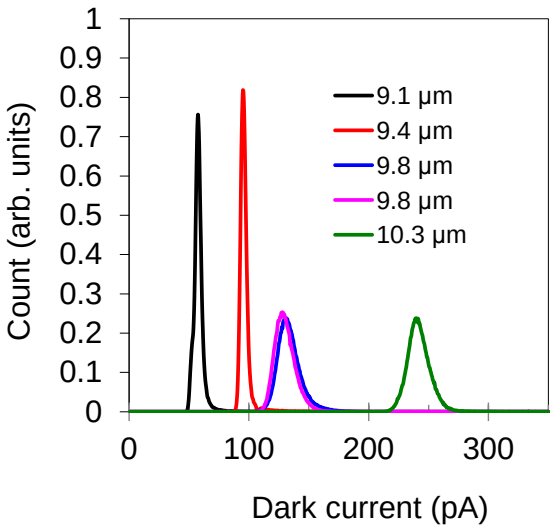

Figure 5. 78 K dark current distribution of five Pelican-D LW FPAs with cut-off wavelengths between 9.1µm and 10.3µm (normalized to constant area)

maximum distribution width is 12%, for the two FPAs with a 9.8µm cut-off, which is still quite narrow. Note that these two FPAs have virtually identical distributions, showing the high reproducibility of our FPA process. None of the distribution curves have a significant high current tail, and their narrow widths demonstrate a high degree of uniformity. A narrow dark current distribution is very good for the stability of the FPA against temperature or bias fluctuations. The median dark current values of all five FPAs are within about one order of magnitude of the dark current range predicted by $Hg_xCd_{1-x}Te$ Rule-07.[6]

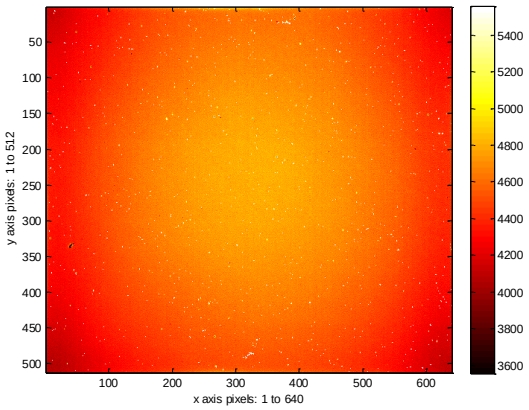

Figure 6. Raw signal map (in Digital levels) registered by the Pelican-D LW FPA, operating at 78K in front of a black body at 35°C.

The good uniformity of our T2SL FPA technology is well demonstrated in Figure 6, which shows a map of the raw signal registered (in digital levels) when the Pelican-D LW FPA is placed in front of a black body at 35°C before any non-uniformity correction has been performed. The map is very uniform, with no stains, large clusters or other variations across its area. This in turn leads to a very low RNU after a two point correction (2PC) is performed. The magenta line in Figure 7 shows a plot of RNU vs. well fill (WF) for this FPA, measured using different black body temperatures and a constant integration time, with a 2PC performed at WF values of 52% and 72% respectively. The RNU remains below 0.02% of the dynamic range for WF values in the range 40 - 80%. Moreover, the FPA is very stable and can maintain a stable image for many hours without any further corrections, as shown by the red line, which was registered one hour after the 2PC was performed. The dashed lines show RNU curves after switching the detector off and then immediately back on (black), or back on the next day (blue), and performing a 1PC .In all cases the RNU curves remain within ~0.01% of the original calibration curve.

At 65% well fill of its $6Me^-$ capacitor and a frame rate of 240Hz, Pelican-D LW offers an NETD of 36mK when configured with F/2.7 optics. By averaging 8 frames at a time, the detector

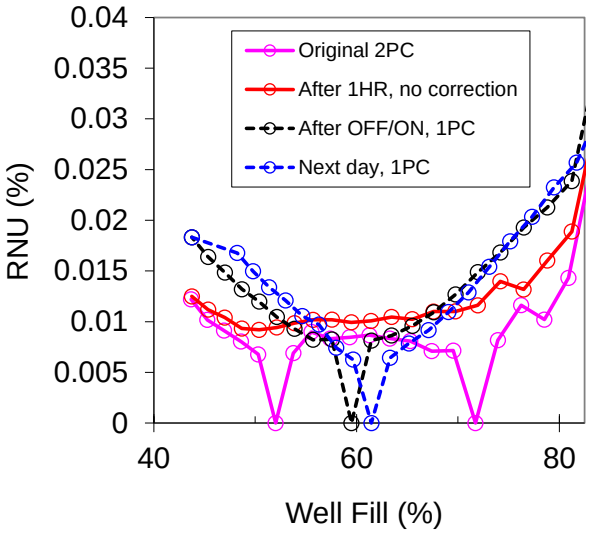

Figure 7. RNU of Pelican-D LW FPA at 78K after performing a two point correction (2PC) at 54% and 72% well fill (magenta); one hour later with no correction (red); After turning off and on with a 1PC; Next day with a 1PC.

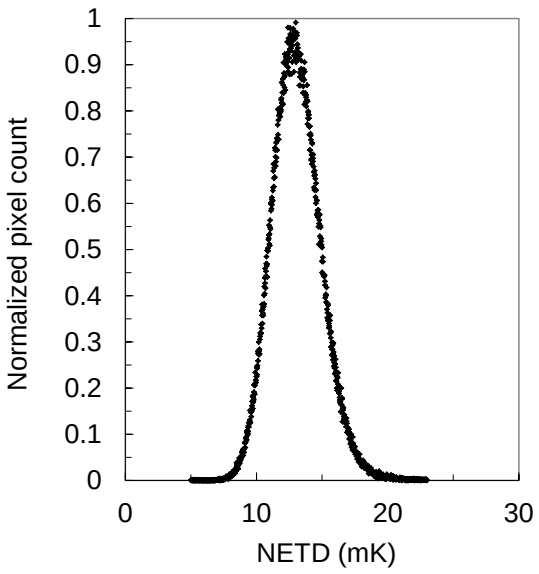

Figure 8. NETD distribution of the Pelican-D LW FPA at 78 K and at a frame rate of 30 Hz

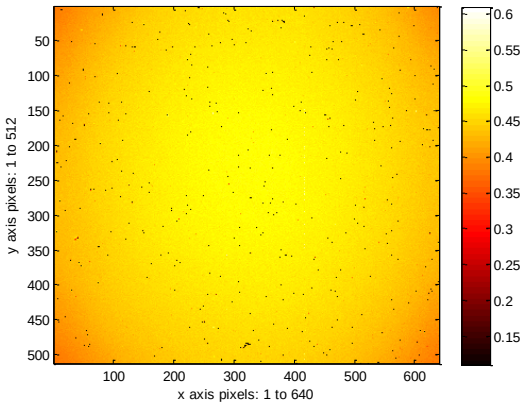

Figure 9. QE Map of the Pelican-D LW FPA operating at 78 K

operates at an effective frame rate of 30 Hz. The NETD distribution measured under these conditions for the Pelican-D LW FPA is shown in Figure 8. The distribution is narrow and symmetric with no pronounced tailing. The peak value is 13 mK which is a reduction of $\sqrt{8}$ relative to the single frame value. This is as expected for pure shot noise, and shows that any noise introduced by the averaging procedure is negligible.

In Figure 9 we show a map of the pixel QE for the same FPA as in Figure 8, in which none of the defective pixels have been removed. The total number of both hard and soft defects on the FPA, defined according to SCD's stringent production

Parameter	Value
Format	640 × 512
Pitch	15 μm
Cut-off wavelength	9.3μm (filter)
Quantum efficiency	> 50%
Operability	> 99%
RNU	< 0.04% STD/DR @ 10 - 90% Well Fill capacity
NETD	15mK @ 65% Well Fill capacity, 30Hz (by averaging 8 frames)
Response Uniformity	< 2.5% (STD/DR)
Electronics	Camera Link
Cooler	Ricor K548
Weight	750 gm
Environmental conditions	-40 to +71°C
Total Power at 23°C	16 W
Cool down time	8 min
MTTF (depends on mission profile)	15,000 hours

Table 2. Appearance of Pelican-D LW IDCA and specification of performance at 77 K

line criteria, is 1446 giving an FPA operability of 99.56% in this case.

In Figure 9, the QE values for each pixel are the average values over the usable LWIR spectral window, defined as the number of photoelectrons measured by the ROIC divided by the number of photons arriving at the detector after passing through a cold filter with a wavelength range of 8 - 9.3 μm and a flat transmission. For the measurement, the detector was placed in front of a black body with a temperature of 35°C. The QE

Figure 10. Image registered with the 15μm pitch, 640 × 512 Pelican-D LW FPA operating with F/2.7 optics at 77K (Scene distance = 5 Km)

map in Figure 9 shows an almost constant value of ~ 48% across the whole FPA, which agrees quite well with the value expected for a one pass detector with the same AL thickness (4.5 μm) discussed in the previous section. If we define the background limited performance (BLIP) temperature as the detector operating temperature at which the dark current is equal to the photocurrent, the QE and dark current results discussed in this section yield a BLIP temperature with F/2.7 optics of 90 K. This is significantly higher than the operating temperature of 77K. At 77K, the dark current is more than 15× smaller than the photocurrent and as noted above, its distribution is narrow, making for good image stability against small temperature fluctuations.

Finally, in Figure 10, we show an image at 5km registered with the Pelican-D LW FPA operating at 77K.

5. CONCLUSIONS

In this article we have presented Pelican-D LW, which is SCD's new LWIR FPA detector. It has a format of 640 × 512 with a 15 μm pitch, and operates at 77K with a nominal detector cut-off wavelength, defined currently by a cold filter, of 9.3 μm. The pixel operability is above 99%, according to SCD's standard production line criteria for the definition of bad pixels. The present version is a single pass detector with a QE of ~48% and exhibits very high uniformity and stability of its response and dark current. The FPA has a very stable RNU below 0.02% of the dynamic range (DR) for well fills between 40 and 80%. The active sensing material is based on a patented diffusion limited XB_0p barrier architecture, where an InAs/GaSb T2SL is used for the AL and an InAs/AlSb T2SL is used for the barrier layer. We have shown that sophisticated simulation techniques exist at SCD which can predict the detector cut-off wavelength and spectral response a-priori, according to the individual layer thicknesses chosen for each superlattice period, and the overall active layer stack thickness. Pelican-D LW demonstrates the versatility of InAs/GaSb as a tunable active layer detector material, and shows that this material can now be considered to be a realistic alternative to $Hg_xCd_{1-x}Te$ for small pitch, high performance LWIR and dual-color FPA detectors

ACKNOWLEDGEMENTS

The authors acknowledge technical support from Mr. S. Greenberg, who was responsible for the smooth operation of the MBE machine, and Ms. H Schanzer, Ms. H. Moshe, Mr. Y. Caracenti, Ms. N. Hazan, Mr. I. Bogoslavski, Mr. Y. Osmo, Mr. M. Keinan, Ms. L Krivolapov, and Ms. M. Menahem who have all contributed to the successful processing, packaging or characterization of the devices.

REFERENCES

[1] G.A. Sai-Halasz, R. Tsu, and L. Esaki, "*A new semiconductor superlattice*" Appl. Phys. Lett. **30**, 651 (1977)

[2] A. Glozman, E. Harush, E. Jacobsohn, O. Klin, P.C. Klipstein, T. Markovitz, V. Nahum, E. Saguy, J. Oiknine-Schlesinger, I. Shtrichman, M. Yassen, B. Yofis, and E. Weiss, "*High performance InAlSb MWIR detectors operating at 100K and beyond*" Proc. SPIE **6206**, 6206-0M (2006)

[3] P.C. Klipstein, *Depletionless Photodiode with Suppressed Dark Current*…, US Patent 7,795,640 (2 July 2003)

[4] P.C. Klipstein, *Unipolar semiconductor photodetector with Suppressed Dark Current*…, US Patent 8,004,012 (6 April 2006)

[5] P.C. Klipstein, "*XBn Barrier Photodetectors for High Sensitivity and High Operating Temperature Infrared Sensors*", Proc. SPIE **6940**, 6940-2U (2008)

[6] W.E. Tennant, "*Rule 07 Revisited: Still a Good Heuristic Predictor of p/n HgCdTe Photodiode Performance?*" Journal of Electronic Materials **39**, 1030 (2010)

[7] P.C. Klipstein, E. Avnon, Y. Benny, R Fraenkel, , A. Glozman, S. Grossman, O. Klin, L. Langoff, Y. Livneh, I Lukomsky, M. Nitzani, L. Shkedy, I. Shtrichman, N. Snapi, A. Tuito and E. Weiss, *InAs/GaSb Type II superlattice barrier devices with a low dark current and a high-quantum efficiency*, Proc. SPIE **9070**, 9070-0U (2014)

[8] P.C. Klipstein, Y. Livneh, A. Glozman, S. Grossman, O. Klin, N. Snapi and E. Weiss, "*Modeling InAs/GaSb and InAs/InAsSb Superlattice Infrared Detectors*", Journal of Electronic Materials, **43**, 2984 (2014)

[9] Y.Livneh, P.C. Klipstein, O. Klin, N. Snapi, S. Grossman, A. Glozman and E. Weiss, "*$k \cdot p$ model for the energy dispersions and absorption spectra of InAs/GaSb type-II superlattices*", Phys. Rev. B **86**, 235311 (2012); Erratum, Phys. Rev. B **90**, 039903 (2014)

[10] PC Klipstein, Y Gross, D Aronov, M Ben Ezra, E Berkowicz, Y Cohen, R Fraenkel, A Glozman, S Grossman, O Klin, I Lukomsky, T Markowitz, L Shkedy, I Shtrichman, N Snapi, A Tuito, M Yassen, E

Weiss "*Low SWaP MWIR detector based on XBn focal plane array*", Proc. SPIE **8704**, 8704-1S (2013)